EPJ Web of Conferences **354**, 04008 (2026) https://doi.org/10.1051/epjconf/202635404008
GCMM 2025

Environmental Impact on Damage Prediction and Structural Response Simulation in Reinforced Concrete Elements

Rajesh A[1], *Sharmilaa* G[1], *Kalyana Chakravarthy* P R[1*]

[1]Department of Mechanical Engineering, VISTAS, India

Abstract. This work developed modeling the environmentally-induced mechanical behavior of reinforced concrete (RC) components, and the aim of structural safety as well as ecological sustainability. Through Finite Element Modeling (FEM), the current RC structures are recreated digitally where the response of the structural building to mechanical and environmental stressors is evaluated. The study focuses on the interplay of corrosion, carbonation, freeze thaw and urban pollutants. The models of damage such as Mazars, Lemaitre and Continuum Damage Mechanics are modified to accommodate material degradation because of exposure on the environment as well as climate change. Four beams of different degrees of damage were experimented in the laboratories and simulations were done using ANSYS 14.5. The framework is used to predict such critical phenomena as crack propagation, strain localization, and fatigue, and provides insight on eco-sensitive deterioration. Simulations are used to derive key performance indicators such as the degradation of stiffness, energy dissipation, failure under sustainable loads, etc. The results are supposed to inform climate-resistant retrofitting programs, which encourage resilient, low impact material and performance evaluation over the long-term. Eventually, this production contributes to the development of sustainable infrastructure management by integrating the environmental concerns into the structural design and maintenance.

1 Introduction

Environmental degradation is a major threat to reinforced concrete (RC) buildings, and highly sophisticated strategies of Simulation-based retrofitting should be developed to boost the resilience and increase the service life. Carbonation, freeze-thaw cycles, seismic activity, and chloride-induced corrosion can be modeled effectively with simulation tools and allow the choice of the proper retrofitting techniques such as fiber-reinforced polymer (FRP) wrapping, concrete jacketing, cathodic protection, as well as ultra-high-performance concrete overlays. This design is cost-effective, resource efficient and consistent with sustainable infrastructural development through reduction of unwarranted demolition and construction [1-3]. The experiments show the effect of corrosion on the RC elements. Axial strain and

* Corresponding author: kalyaniponnayya@gmail.com

load-bearing capacity of 50 specimens (150 mm diameter, 300 mm height) that was subjected to accelerated corrosion with 6V power found it to be low [1]. Prolonged exposure to sulfate and chloride solution (1200 days, 5% NaCl, 0-4% sulfate) showed that the corrosion current density of blended cement was much lower than that of plain cement [2]. High-quality composite materials were able to repair sulfate-inflicted beams using different FRP setups [4].

Finite element and machine learning have enhanced damage prediction. Models based on LSTMs provide an accurate prediction of bending moments in fire-damaged RC beams reinforced with CFRP sheets [5, 6] and enhanced the predictions of mid-span displacement and the degree of damage using the models under the influence of blast loads [7, 8]. FEM simulators associate change in seasonal temperature with corrosion detection in RC elements through Acoustic Emission [9, 10]. Temperature, ohmic resistance, duration of corrosion, and chloride concentration were determined as important factors by non-linear regression that have impact on service condition corrosion [11 - 15]. Recent developments also combine the fracture mechanics and progressive cracking theory with ANSYS [16-17], and have been applied to a wide range of structural members such as columns, beams, beam-column joints, shear walls, and nuclear power plant structures [18].

2 Materials and Methods

2.1 Proposed Methodology

The study uses a multi-scale simulation that uses a complex mix of highly developed numerical modeling with experimental validation to evaluate the behavior of degradation and damages in RC structures under extreme environmental and mechanical forces [19, 20]. The 3D Finite Element Model (FEM) of high fidelity developed in ANSYS 14.5 takes into consideration the heterogeneity of concrete and the reinforcement of steel embedded within it and replicates the geometric, material, and boundary conditions of RC components. Fracture models and continuum Damage Mechanics (CDM) System and plasticity Fracture models are simulations of progressive cracking, loss of stiffness and failure caused by monotonic and cyclic loading [21]. The effects of time-dependent degradation functions on the mechanical properties such as bond-slip relations, elastic modulus, and energy dissipation ability are added to the corrosion of the environment; namely, the effects of chloride penetration, carbonation, infiltration of urban pollutants, exposure to sulfates, and freeze-thaw cycles. Structural response to explosive impact is modeled by dynamic situations in which the load of implosion has variable parameters (charge weight, detonation location, reinforcement ratios) [22]. Thorough logs such as failure probabilities, stiffness reduction, crack propagation measures, and performance indicators left after the blast-impact test are documented and checked with reference to benchmark blast-impact test outcomes, frequency-power spectral density (PSD) analysis, acceleration measurements, and observation of crack patterns.

2.2 Geometry and Mesh Generation

The geometric layout contains a 10 story RC structure (11,200 mm x 10,200 mm plan, 31,050 mm height) with typical spacing of floor plans of 2,200 mm x 3,300 mm, beam sections of 400 mm x 200 mm with longitudinal bar reinforcement (4Ph16 mm) and transverse reinforcement (Ph8 mm) at 250 mm intervals, column sections of 400 mm x 400 mm, longitudinal reinforcement. Figure 1 shows the overall construction description of a ten-story reinforced concrete building, with part (a) depicting the complete 3D geometric construct

having a plan dimension of 11200 mm x 10200 mm and a full height of 310500 mm: part (b) illustrates the overall floor plan with slab panels that are separated by 2200 mm x 3300 mm and identifying the critical analysis points (A, B, C and D) at the mid-span areas; part (c) and (d)

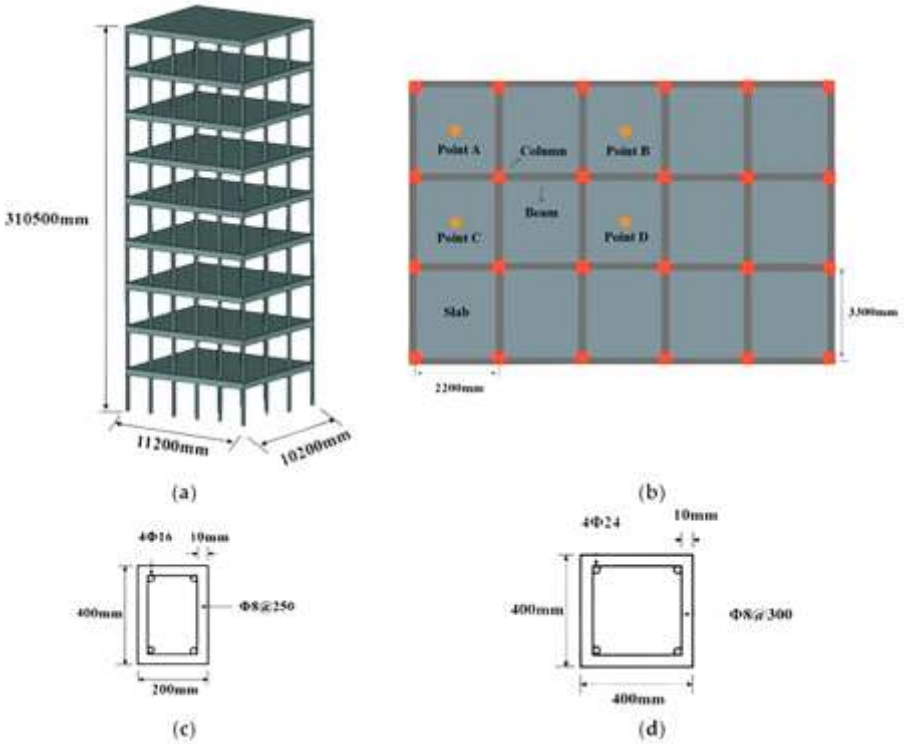

Fig. 1. Geometric layout and computational finite-element model

2.3 3D FEM Modeling

Steel reinforcement also makes use of Beam161 elements that capture three-dimensional behaviour that includes the axial loads, dual axis bending and the large deformations conditions with finite strain behaviour as it is characteristic of reinforcement bars. Beam161 elements use circular cross-sectional profiles which are set-up using ANSYS 14.5 section type panels is shown in the figure 2. Solid164 elements (3D solid types with eight nodes that provide nine degrees of freedom of translational motion, acceleration, and velocity along X, Y, and Z, respectively) are used in concrete matrix, surrounding air, and dynamic explosive interactions. This model incorporates geometrical accuracy, material heterogeneity, nonlinear constitutive models such as cracking, crushing, yielding and post yield softening and bond-slip interaction between the concrete and reinforcement.

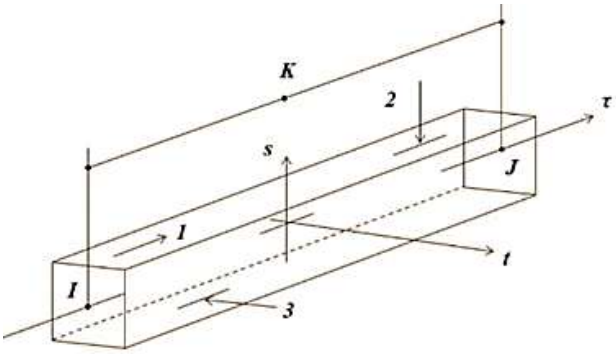

Fig. 2 Schematic diagram of Beam

Table 1. Geometry and Mesh Parameters of RC Elements

Parameter	Value
Concrete block dimensions	1000 mm × 250 mm × 250 mm
Longitudinal reinforcement	4 bars of 16 mm diameter
Transverse reinforcement (ties)	8 mm diameter @ 100 mm c/c
Concrete cover	25 mm
Element type	C3D8R (8-node brick)
Average element size (concrete)	15 mm
Average element size (steel)	10 mm

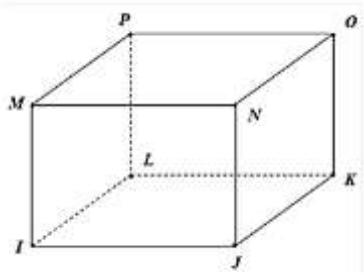

Fig. 3 Schematic diagram of Solid164 unit (ANSYS 14.5)

It is an element of a three-dimensional solid type used to represent volumetric elements of structural models in a discrete way. The Solid164 element has eight nodes, each with 9 degrees of freedom, which consider the X, Y, and Z acceleration, velocity, and translation as shown in Figure 3.

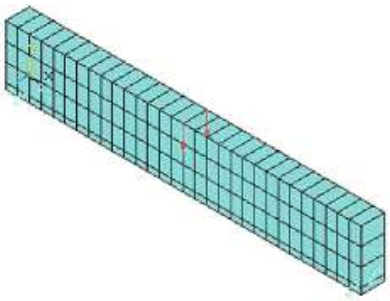

Fig. 4 Finite element model and boundary conditions

The RC model is constructed in such a way that it incorporates geometric accuracy, realistic modeling of material heterogeneity and contains discrete concrete and steel reinforcement areas and this is illustrated in figure 4. The implementation of advanced constitutive models is done to account nonlinear behavior, such as cracking, crushing, yielding, and post-yield softening, and bond-slip interaction between the concrete and reinforcement.

3 Numerical Modeling Parameters

3.1 Corrosion-Induced Expansion

Corrosion of steel reinforcement generates expansive pressure on neighboring concrete to crack and delaminate. Volumetric expansion is considered as an internal pressure acting radially on steel bars and depth of corrosion penetration is determined by a law by Faraday.

$$x\_corr(t) = (i\_corr \times M \times t) / (n \times F \times \rho) \quad (1)$$

x_corr(t) represents corrosion depth, i_corr represents corrosion current density, M is iron molar mass, 3 represents steel density, n represents valence number and 'F' Faraday constant. Figure 5 analysed the numerical analysis model of the RC beam, the pressure p_corr due to corrosion is applied as:

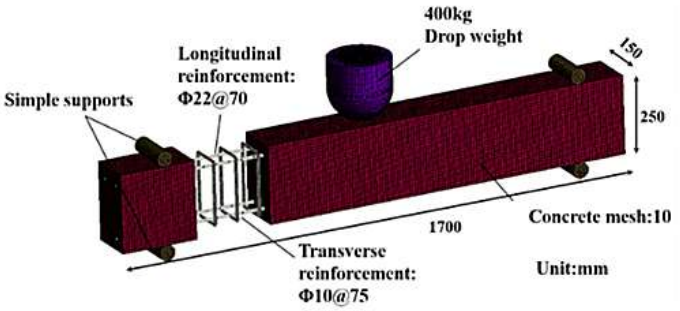

Fig. 5 Numerical analysis model of the RC beam

$$p\_corr = k \times x\_corr(t) \quad (2)$$

where 'k' is an empirical constant from experimental results.

3.2 Carbonation and pH Reduction

Carbonation decreases the alkalinity of concrete, which causes corrosion of the reinforcement. The depth of carbonation is in accordance with the second law of Fick.

$$x\_c = K\_c \times \sqrt{t} \quad (3)$$

with x_c carbonation depth and K_c carbonation coefficient. pH drop at depth of reinforcement is connected to depassivation potential:

$$pH(x\_c) = pH_0 \times e^{(-\alpha \times x\_c)} \quad (4)$$

where α is a decay factor based on concrete composition.

3.3 Freeze-Thaw and Urban Pollutant Modeling

Freeze-thaw cycles induce microcracking of volumetric expansion of pore water, which is modelled as alternating internal thermal pressures with strain incremented with time:

$$\varepsilon\_ft = \beta \times N \quad (5)$$

Where 'ε_ft' is cumulative freeze-thaw strain, N is the number of cycles and 8 is the material specific coefficient. Cycle dependent degradation of elastic modulus:

$$E(N) = E_0 \times e^{(-\gamma N)} \quad (6)$$

The chemical and physical degradation are caused by urban pollutants (chlorides, sulfates). Chloride ingress is in accordance to the first law of Fick:

$$C(x,t) = C\_s \times (1 - \mathrm{erf}(x / (2\sqrt{(D\_cl \times t)}))) \quad (7)$$

C(x,t) is the chloride concentration in the depth of x, Cs is the chloride concentration on the surface, and D_cl is the diffusion coefficient.

3.4 Damage Constitutive Laws

The laws of advanced damage are simulators of progressive RC damage due to mechanical and environmental forces. Mazars Damage Model the Mazars Damage Model model of micro-crack initiation and propagation under tensile loading using isotropic scalar damage variable d:

$$\sigma = (1 - d) \times C : \varepsilon \quad (8)$$

Where, C is an elasticity tensor and ε is a strain tensor. The Lemaitre Plastic Damage Model integrates damage that is plastic with isotropic damage, and this model represents permanent deformation and the degradation of microstructures because of damage evolution dependent upon equivalent plastic strain. Continuum Damage Mechanics (CDM) combines anisotropic damage and thermodynamic consistency, where damage is a tensorial quantity, which develops with respect to energy release rates. These models are coupled with the environmental parameters (corrosion induced strain, depth of carbonation, freeze thaw cycling) and can be used to make time-dependent degradation embedded in the mechanical response equations.

3.5 Structural Response Simulation

Structural response evaluation is the multi-scale numeric method of crack propagation modeling, strain localization, and fatigue life evaluation in realistic environmental

conditions. Smeared crack approach is used in crack propagation of distributed micro-cracking and cohesive crack model of localized failure zones. Fracture energy G f controls energy necessary to extend crack, and is included in element deletion or traction-separation laws. Strain localization Non-local averaging or gradient-enhanced damage formulations make strain localization free of mesh dependency and enhance numerical stability. Under cyclic loading: Fatigue behavior Fatigue behavior under cyclic loading simulates with laws of accumulation of damage:

$$D = \Sigma(n\_i / N\_i) \quad (9)$$

Where D is cumulative damage, n i is number of cycles of stress level and N i is number of cycles to failure. Time-dependent deterioration assesses using the temporal degradation functionality of material properties such as stiffness, strength, and ductility, to describe long-run loss of structural integrity.

3.6 Performance Indicators

Evaluations performance Performance evaluation uses quantitative parameters of simulation results, Energy dissipation capacity:

$$E\_d = \int F \times d\Delta \quad (10)$$

Where F is force and Δ displacement. Stiffness degradation:

$$K(t) = K_0 \times (1 - D(t)) \quad (11)$$

Likely failure with reliability index formulation:

$$\beta = (\mu\_R - \mu\_S) / \sqrt{(\sigma\_R^2 + \sigma\_S^2)} \quad (12)$$

where μ R and s R, s S are resistance and load effect means and standard deviations. Deterioration model and serviceability limit state Life-cycle performance indicators:

$$t\_service = t\_crit \times \ln(1 / (1 - D\_limit)) \quad (13)$$

These measures provide a strong structural resiliency evaluation, which provides viable design and retrofitting plans of infrastructure affected by climate changes.

4 Results and Discussion

4.1 Energy Dissipation Analysis

The comparative analysis of energy dissipation with different environmental loading conditions showed a substantial deterioration in the performance. Table 2 showed the comparative study on energy dissipation in reinforced concrete (RC) elements under different environmental loading conditions. The best performance was observed with the baseline specimens (325 kN load, 10.2 mm displacement, 2,485 kNmm energy dissipation). Exposure to corrosion had a minor effect on the maximum load with a decrease in maximum load with increase in displacement (11.5 mm) and minimally decreased energy dissipation (2,456 kNmm). Weaknesses in structural response were also caused by carbonation (295 kN load, 12.3 mm displacement, 2,405 kNmm energy dissipation). Severe degradation (280 kN load, 13.8 mm displacement, 2,330 kN.mm energy dissipation) was caused by freeze-thaw cycles. Strong effects (270kN load, 14.1 mm displacement, 2,295 kN mm energy dissipation) were observed on the pollutants of the environment. The cumulative adverse effects on the structural integrity and energy capture ability were demonstrated through combined

environmental effects that were of critical deterioration (245 kN load, 15.5 mm displacement, 2,165 kN/mm energy dissipation).

Table 2. Energy Dissipation Under Different Environmental Loads

Scenario	Max Load (kN)	Displacement (mm)	Energy Dissipation (kN·mm)
Baseline	325	10.2	2485
Corrosion	310	11.5	2456
Carbonation	295	12.3	2405
Freeze-Thaw	280	13.8	2330
Pollutants	270	14.1	2295
Combined Effects	245	15.5	2165

4.2 Structural Damage Characteristics

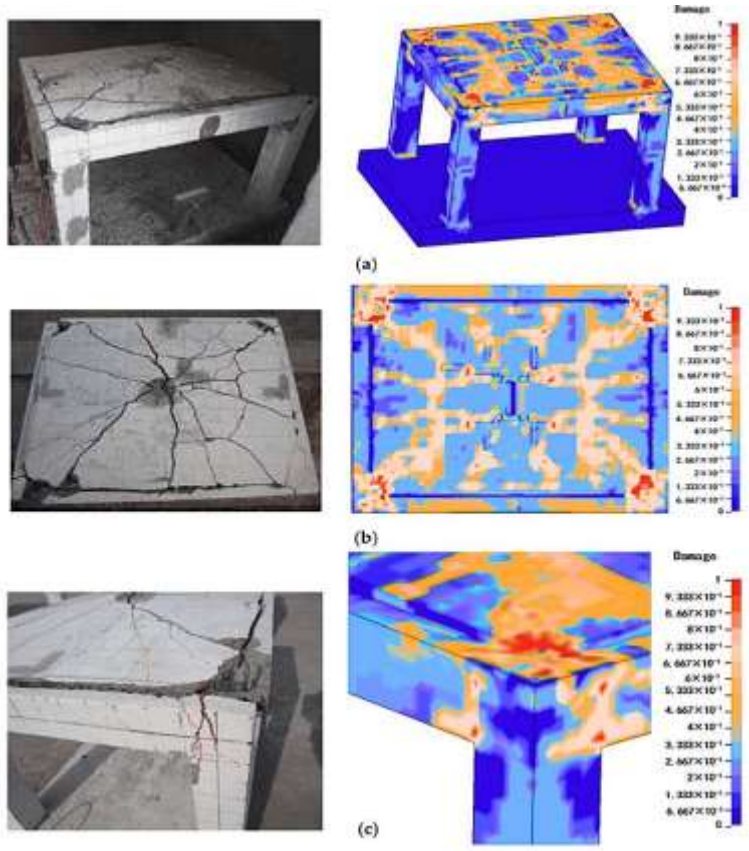

Fig.6 Structural damage of 200 g emulsion explosive detonation: (a) full frame response; (b) localized failure at the slab surface; (c) concentration of the damage at the beam column joint

The structural components exposed to 200 g emulsion explosion detonation were severely cracked and spalled using concrete especially in corners and upper slabs. Simulation results (finite element) were shown to represent the damage distribution with the presence of stress concentration areas at column-slab intersection and the slab centre as reflected by large damage indices approaching 0.9. Simulations had a high replication of radial and circumferential crack patterns originating at the points of blast as symmetrical damage propagation. Beam joints exhibited high levels of concrete fragmentation and joint failure with localized levels of damage severity at slab-column interfaces and showed that damage models based on FEM-based approaches were good in the spatial distributions and severity of the structural degradation caused by the blast. figure 6 (b) is about the top of the frame which indicates radial and circumferential crack patterns generated at the center of the blast in the experimental image which is well reproduced in the simulation as localized high damage intensities at the slab-column interface. Figure 6 (c) highlights the beam joint that is depicted with a substantial fragmentation and joint failure in the physical test and reproduced in the simulation with the same localized damage intensities at the slab-column interface. Comparison of all subfigures shows how the FEM-based damage model could be successful in the spatial distribution and acuity of the structural degradation of the blast damage.

4.3 Stiffness Analysis

Table 3 showed how the stiffness of reinforced concrete (RC) elements was deteriorating with time (25 years) in continuous environmental conditions. In the first stage (Year 0), the elastic modulus was measured at 30, 000 Mpa, which was the base, and no measures of reduction were done. This resulted in a decrease in the modulus of 25,821 Mpa (13.93 percent) after five years implying that microstructural deterioration had occurred at a very young age. At the 10 years mark stiffness had reduced further to 2222224 Mpa which is equivalent to 25.92 reduction in stiffness which is the cumulative effect of environmental stressors. At 15 years of age the elastic modulus lowered further to 19,128 Mpa by a margin of 36.24 indicating that significant damage was done to the material matrix. The initial level of 16,464 Mpa was minimized to 16,464MPa in 20 years which shows a reduction of 45.12 in the initial figure, which is evidence of the advanced material weakening. The elastic modulus has decreased to the lowest point of 14,170 Mpa at the end of the 25 years exposure time, which is a significant drop of 52.76 percentage of the stiffness. These results in Table 3 confirmed the constant and harsh degradation tendency with time passing, which accentuates the susceptibility of RC structures to environmental influences and the seriousness of the need to implement preventive actions and maintenance in a timely manner.

Table 3. Stiffness Degradation Over Time Under Environmental Exposure

Time (Years)	Elastic Modulus (MPa)	Reduction (%)
0	30000	0.00
5	25821	13.93
10	22224	25.92
15	19128	36.24
20	16464	45.12
25	14170	52.76

4.4 Chloride Ingress and Corrosion Depth Prediction

The correlation between the ingress of chloride at different depths of concrete and the corrosion depth which is predicted according to these readings are shown in Table 4 and it shows a gradual increase in the penetration of chlorides and its effects on the corrosion of the steel reinforcement. The highest concentration of the chloride was 0.3033 kg/m^3 of the solution at the shallow depth of 5 mm, and the correspondingly small value of the predicted corrosion depth was 0.0506 mm, showing early surface impurity. At depths of 10 mm, the chloride concentration was 0.1839 kg/m^3, which is less than predicted corrosion depth 0.1004 mm, and the corrosion potential was gradually increasing with depth even though the chloride concentration was declining. The depth continued to decrease in consecutive depths where chloride concentration gradually reduced to 0.0249 kg/m^3 at 30 mm, and predicted corrosion depth gradually rose to 0.3000 mm at the same depth. The evidence shows that there is a negative correlation between the depth of corrosion and the chloride concentration at the distance of surface, which indicates long-term potential of reinforcement corrosion in the presence of long-term chloride ingress, although at lower concentrations at a greater distance in the concrete. This trend implies that the level of chlorides increases with time at the reinforcement level such that even low levels are capable of causing extensive corrosion once the critical level is surpassed.

Table 4. Chloride Ingress and Corrosion Depth Prediction

Depth (mm)	Chloride Concentration (kg/m³)	Predicted Corrosion Depth (mm)
5	0.3033	0.0506
10	0.1839	0.1004
15	0.1116	0.1502
20	0.0677	0.2001
25	0.0410	0.2501
30	0.0249	0.3000

4.5 Damage Process of RC Frame Under Internal Explosion Load

The time-history graphs of mid-span displacement of reinforced concrete beams under two loading sequences impacts-blast and blast-impact are shown in figure 7, with an impact velocity of 6.86 m/s and scaled distance Z = 0.32 m/kg^1/kg/3. During the first stage (0 0.022 s), which is single loading, the two curves exhibit a drastic decline, and the impact-blast sequence is at about -0.015 m and the blast-impact sequence at about -0.017 m. Following the change to combined loading outside the range of 0.022 s, the magnitude of the displacement in the impact-blast case grows very rapidly, reaching values of the order of -0.032 m towards 0.03 s, showing a more violent structural response. On the other hand, the case of the blast-impact has a more controlled fluctuation, and the displacement approaches -0.020 m. The general tendency is that the

effect-blast sequence causes bigger mid-span deflection and dynamic instability than the blast-impact sequence, indicating that the loading sequence plays an important role in the deformation and destruction properties of RC beams. This observation means that the structures that are impacted before the blast undergo more severe deformation because the initial impact may make the beam less robust and exposed to the latter loading of the blast. Conversely, in a case where the blast is initially experienced, there are chances that the beam will experience more residual capacity to withstand impact perhaps because of other forms of energy dissipation, or stress distributions.

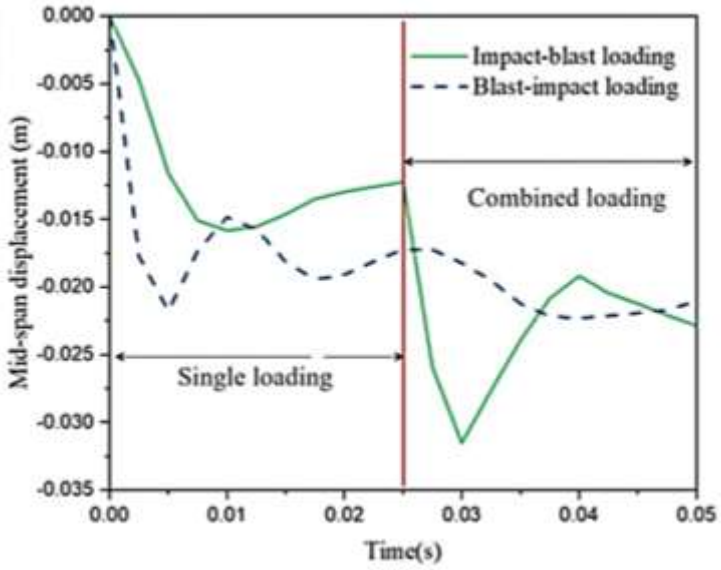

Fig. 7 Mid-Span displacement Time-History under different loading sequences

The table 5 shows how the structures of reinforced concrete (RC) have gradually declined in strength with the service lifespan of 25 years and exposure to environmental forces. The residual performance index is at its highest value of 1.00 at the onset of the service life (0 years), meaning that there is no deterioration. Nevertheless, with time, this index decreases slowly with time as the environment is damaged over time through corrosion, carbonation, and freeze-thaw effects. In the 5 th year, the performance index is at 0.85, which is associated with 15 percent structural weakening. This decline is constant, 0.70 at 10 years (30% deteriorated), 0.55 at 15 years (45%), and 0.40 at 20 years (60%). The index of residual performance decreases drastically to 0.25 at the end of 25 years implying the loss of 75 percent of structural integrity. This tendency highlights the role of maintenance in time, creation of monitoring and possible retrofitting in order to guarantee long-term structural safety and service in non-favorable environmental conditions. The increasing rate of degradation, especially in later life, indicates that the processes that produce damage, e.g. corrosion, might increase with time, forming nonlinear degradation curves that need proactive management beyond reaching a critical point.

Table 5. Life-Cycle Residual Performance Index

Service Time (Years)	Residual Performance Index	Structural Deterioration (%)
0	1.00	0.0
5	0.85	15.0
10	0.70	30.0
15	0.55	45.0
20	0.40	60.0
25	0.25	75.0

4.6 SIMULATION RESULTS

The ANSYS designed model simulations of concrete beams depicts a cumulative process of crack and collapse mechanisms with the growing loads of the structure. Beams at lower loads (41-49 kN) show a mixture of both diagonal shear cracks at the support and vertical flexural cracks in the mid-span indicating that both shear and tensile failures are present. With further increase in loading to ultimate capacity (68-120 kN) the crack patterns become more intricate and focused with heavy concentrations of red markers, indicating locations of severe damage where crushing and widespread cracking results in ultimate failure. The visualizations with color coded data are especially effective in separating between the types of cracks and the level of severity so that the researcher can determine how failure shifts between the initial shear cracking and flexural cracking to the ultimate degradation of the material. Such a progressive development manifests how the structural responses of the beams change due to initial damage up to the final collapse and proves the simulation capacity of the realistic failure process in reinforced concrete elements.

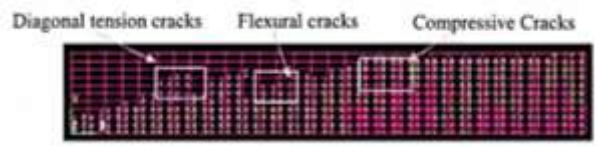

Fig. 8 Integration of all cracks at 49.00kN for concrete Beam

4.7 Comparison and Verification of Structural Dynamic Response

Figure 9 in the image presents a dynamic response of a structure under 200g of emulsion explosives loading, comparing experimental data to simulation results in four sub-plots. The sub-plots (a) and (b) show acceleration verses time. Figure (a) is a plot of acceleration (g) versus time (μs) which indicates that, at the beginning of the process, high-frequency oscillations with peaks of about 6000 g to 8000 g in both test and simulation rise and at 1000 μs, the oscillation decays to nearly zero. There is also acceleration (g) vs. time (ms) in sub-plot (b) which has initial high peaks of approximately 12000 g and -6000 g that rapidly decays reaching a constant value of 0 g at about 2000 ms. The Power Spectral Density (PSD) versus frequency (Hz) is shown in sub-plots (c) and (d).

The PSD of the values in (Fig. 9.c), which are the distribution of power per unit of frequency, exhibit high peaks of both test and simulation, especially between 0 Hz and 10,000 Hz, with additional high peaks around 25,000 Hz and 40,000 Hz, indicating that the major frequencies in the structural response lie between these regions. Sub-plot (Fig. 9.d) is another PSD v versus frequency plot, but the PSD values peak at the start with values of over 300 with the test data and about 200 with the simulation and then drops off rapidly thereafter after 5000 Hz and the rest of the higher frequencies are relatively low indicating that the power tends to be concentrated in the lower frequency range. All these graphs indicate an excellent overall correspondence in the simulated and experimental dynamic response of the structure, especially in the first acceleration peaks and the general frequency content, although a few differences exist in the magnitudes of the peaks and their distribution in a specific frequency.

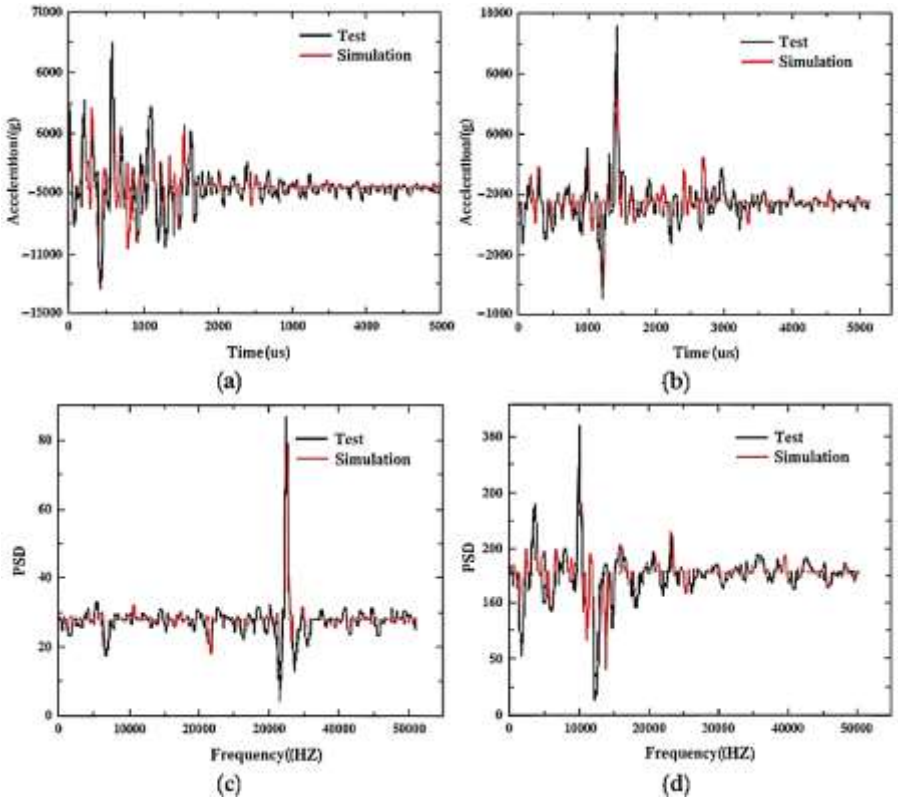

Fig. 9 Dynamic response of a structure under the action of 200 g of emulsion explosives: (a) acceleration response curve of A2; (b) acceleration response curve of A3; (c) the frequency–power spectral density curve of A2; (d) the frequency–power spectral density curve of A3..

4.8 Comparative Analysis of Experimental vs Numerical

The ultimate load and mid-span deflection were compared in Table 6 between four reinforced concrete beams (CB1-CB4) under both experimental and numerical (ANSYS) testing. In the case with Beam CB1, the final load observed experimentally was 41.25 kN, which is very close to the ANSYS output of 41.00 kN. The experimental and numerical mid-span deflection was 21.13 mm and 21.75 mm respectively. Beam CB2 had greater load bearing capacity where experimental and numerical values were 69.00 kN and 68.00 kN respectively and deflection values were 8.35 mm and 8.263 mm respectively.

Table 6. Comparative analysis

Beam ID	Ultimate Load (kN)		Deflection at Mid Span (mm)	
	Experimental	Numerical (ANSYS)	Experimental	Numerical (ANSYS)
CB1	41.25	41.00	21.13	21.75
CB2	69.00	68.00	8.35	8.263
CB3	49.50	49.00	20.13	20.83
CB4	125.00	120.00	86.25	87.85

In the case of CB3, the ultimate load was found to be 49.50 kN in the experimental, and 49.00 kN in the ANSYS 14.5 simulation, the results of deflections were 20.13 mm and 20.83 mm. Beam CB4 had the largest load bearing capacity with the experiment registering 125.00 kN and ANSYS 14.5 registering 120.00 kN. It had an experimental mid-span deflection of 86.25 mm and ANSYS 14.5 of 87.85 mm. The high degree of agreement between both experimental and numerical values in all the beams as presented in table 6 confirmed the level of accuracy and reliability of the ANSYS model in its ability to simulate both the strength and deformation behavior.

5 Conclusions

This study was able to construct an elaborate framework of modeling the effects of the environment on reinforced concrete structural behavior, and the correlation of finite element with damage mechanics which can predict the performance of the construction when subjected to both mechanical and environmental overloading. Key findings include

- Sequences of progressive degradation that were well measured in various environmental exposure conditions, and joint action effects reaching to 52.76% reduction in stiffness of 25 years.
- The amount of energy dissipation dropped to 2,165 kN mm (combined effects) compared to 2,485 kN mm (baseline) indicating the important loss of structure resilience.
- The analysis of blast loading showed that there are an important dependence of the reinforcement ratio and the weight of charges, and the displacement grows exponentially as the power of the blast increases.
- The crack propagation modeling was able to predict the progression of failure since the beginning of the initiation up to the stage of severe degradation.
- Reliability indices decreased (3.16 on a normal environment) to almost zero (interaction of environmental factors), which focuses on very critical vulnerability to various concurrent stressors.

The tested and proven simulation modeling system is a strong diagnostic system to assess and retrofit old-fashioned RC infrastructure, which can be used to support climate-adaptable design planning and long-lasting infrastructure operation. Further studies are necessary to come up with adaptive maintenance procedures grounded on real-time environmental testing and extending the model to cover new materials and retrofitting technologies to improve long-term operation in evolving climatic conditions.

References

1. Ahmad, N., Rizwan, M., Ilyas, B., Hussain, S., Khan, M. U., Shakeel, H., & Ahmad, M. E, Nonlinear Modeling of RC Substandard Beam–Column Joints for Building Response Analysis in Support of Seismic Risk Assessment and Loss Estimation. Buildings, 12(10), 1758 (2022)
2. Almustafa, M. K., & Nehdi, M. L, Novel hybrid machine learning approach for predicting structural response of RC beams under blast loading. In Structures (Vol. 39, pp. 1092-1106). Elsevier (2022).
3. Zhang, T., Hou, Z., Chen, Q., Li, X., Fang, Y., Zhang, S., & Sun, W, A novel damage model integrated into the elastoplastic constitutive model and numerical simulations of reinforced concrete structures under cyclic loading. Journal of Building Engineering, 84, 108670 (2024)
4. Liu, Y., Sun, B., Guo, T., & Li, Z, Multiscale damage analysis of engineering structures from material level to structural level: a systematic review. International Journal of Structural Integrity, 16(2), 275-310 (2025)
5. Ahmed, B., Mangalathu, S., & Jeon, J. S, Seismic damage state predictions of reinforced concrete structures using stacked long short-term memory neural networks. Journal of Building Engineering, 46, 103737 (2022)
6. Peng, J. Z., Pan, L. J., Wang, Z. Q., Gao, G. F., Wang, M., Hu, J., ... & Wu, W. T, Self-adaptive graph neural network for predicting blast-induced damage in RC columns across multiple scenarios. Engineering Structures, 337, 120505 (2025)
7. Tran, P. L., Tran, V. L., & Kim, J. K, Mid-span displacement and damage degree predictions of RC beams under blast loading using machine learning-based models. In Structures (Vol. 65, p. 106702). Elsevier (2024)
8. Luo, H., & Paal, S. G, Data-driven seismic response prediction of structural components. Earthquake Spectra, 38(2), 1382-1416 (2022)
9. Anas, S. M., Alam, M., & Saidani, M, Prediction of impact response of square reinforced concrete (RC) slab with square/circular opening under drop-weight impact using FEM simulation. Asian Journal of Civil Engineering, 25(2), 2189-2208 (2024)
10. Song, X., Cheng, X., Li, Y., Guo, R., Zhang, H., Liang, Z., & Wang, S, A numerical model database for rapid seismic damage assessment of typical regular reinforced concrete frame structures in urban building clusters. Journal of Building Engineering, 90, 109392 (2024)
11. Zhang, C., Wen, W., Zhai, C., Jia, J., & Zhou, B, Structural nonlinear seismic time-history response prediction of urban-scale reinforced concrete frames based on deep learning. Engineering Structures, 317, 118702 (2024)
12. Wen, W., Zhang, C., & Zhai, C, Rapid seismic response prediction of RC frames based on deep learning and limited building information. Engineering Structures, 267, 114638, (2022)
13. Vrijdaghs, R., & Verstrynge, E, Probabilistic structural analysis of a real-life corroding concrete bridge girder incorporating stochastic material and damage variables in a finite element approach. Engineering Structures, 254, 113831 (2022)
14. He, J., Gao, R., & Chen, J, A sparse data-driven stochastic damage model for seismic reliability assessment of reinforced concrete structures. Reliability Engineering & System Safety, 223, 108510 (2022)

15. Xu, J. G., Feng, D. C., Mangalathu, S., & Jeon, J. S, Data-driven rapid damage evaluation for life-cycle seismic assessment of regional reinforced concrete bridges. Earthquake Engineering & Structural Dynamics, 51(11), 2730-2751 (2022)
16. Verma, I., Gautam, L., Gomkale, S., Goyal, A., Berwal, P., Al Asmari, A. F., & Islam, S, Structural response of beam-column joint made of fiber reinforced concrete (FRC) using ANSYS FEA simulation. Rocz. Ochr. Środowiska, 27, 174-195 (2025)
17. Nasrul, K. B. M., Radzi, N. A. M., & Hamid, R, Simulation-based evaluation of reinforcement corrosion impact on the flexural performance of RC beams. Journal of Building Pathology and Rehabilitation, 10(1), 41 (2025)
18. Osman, B. H, Experimental study on the behavior of pre-loaded reinforced concrete (RC) deep beams with openings strengthened with FRP sheets. World Journal of Engineering, 22(1), 148-159 (2025)
19. Shelgaonkar, T., & Khante, S, Crack simulation and monitoring of beam-column joint by EMI technique using ANSYS. In Recent Trends in Construction Technology and Management: Select Proceedings of ACTM 2021 (pp. 1101-1113). Singapore: Springer Nature Singapore (2022)
20. Nwankwo, C. O., & Mahachi, J, Analytical and numerical approaches in predicting the flexural behaviour of reinforced concrete beams. In The International Conference on Net-Zero Civil Infrastructures: Innovations in Materials, Structures, and Management Practices (NTZR) (pp. 1423-1435). Cham: Springer Nature Switzerland (2024)
21. Zhang, C., Zhao, Y., Wu, G., Wu, H., Ding, H., Yu, J., & Wan, R, A correlation analysis-based structural load estimation method for RC beams using machine vision and numerical simulation. Buildings, 15(2), 207 (2025)
22. Waqas, R. M., Elahi, A., & Kırgız, M. S, Experimental and finite element analysis of shear deficient of reinforced concrete beam retrofitted externally with carbon fiber reinforced polymer sheet. In Structures (Vol. 72, p. 108232). Elsevier (2025)